

Received: 10 May 2023 / Accepted: 01 June 2023 / Published online: 05 June 2023

*industrial robots, double encoders,
force-torque estimation*

Eckart UHLMANN^{1,2},
Mitchel POLTE^{1,2},
Julian BLUMBERG^{1*}

ESTIMATION OF EXTERNAL FORCE-TORQUE VECTOR BASED ON DOUBLE ENCODERS OF INDUSTRIAL ROBOTS USING A HYBRID GAUSSIAN PROCESS REGRESSION AND JOINT STIFFNESS MODEL

Industrial robots are increasingly used in industry for contact-based manufacturing processes such as milling and forming. In order to meet part tolerances, it is mandatory to compensate tool deflections caused by the external force-torque vector. However, using a third-party measuring device for sensing the external force-torque vector lowers the cost efficiency. Novel industrial robots are increasingly equipped with double encoders, in order to compensate deviations caused by the gearboxes. This paper proposes a method for the usage of such double encoders to estimate the external force-torque vector acting at the tool centre point of an industrial robot. Therefore, the joint elasticities of a six revolute joint industrial robot are identified in terms of piecewise linear functions based on the angular deviations at the double encoders when an external force-torque vector is applied. Further, initial deviations between the encoder values caused by gravitational forces and friction are modelled with a Gaussian process regression. Combining both methods to a hybrid model enables the estimation of external force-torque vectors solely based on measurements of the joint angles of secondary encoders. Based on the proposed method, additional measurement equipment can be saved, which reduces investment costs and improves robot dynamics.

1. INTRODUCTION

Automation and accuracy enhancement methods in robot-based manufacturing often rely on force or pose control under consideration of the external force-torque vector \mathbf{W} acting at the tool centre point (TCP) [1, 2]. On an industrial level the external force-torque vector \mathbf{W} is in general measured directly with a force-torque sensor mounted between the end-effector and the flange of the industrial robot. However, depending on the sensing principle such sensors are accompanied by different disadvantages such as sensitivity to noise, temperature changes, humidity and electromagnetic interference, high power consumption, drift due to static forces or torques, overload vulnerability and loading-unloading hysteresis [3]. Independent of the sensing principle they further suffer from high cost, additional mass and

¹ Institute for Machine Tools and Factory Management IWF, TU Berlin, Germany

² Institute for Production Systems and Design Technology IPK, Fraunhofer, Germany

* E-Mail: blumberg@iwf.tu-berlin.de
<https://doi.org/10.36897/jme/167359>

the lack of sensing an external force-torque vector \mathbf{W} that is not applied to the end-effector. In order to overcome these downsides different alternative approaches to access the external force-torque vector \mathbf{W} have been proposed.

Phong et al. [4] installed additional torque sensors directly at the output side of each joint, which however changes the overall dynamics of the robot and induces compliance. Other researchers proposed methods, which do not rely on additional measurement equipment [5, 6]. The approaches use a disturbance observer, which estimates the external force-torque vector \mathbf{W} based on joint angles \mathbf{q} , velocities $\dot{\mathbf{q}}$, accelerations $\ddot{\mathbf{q}}$ as well as motor currents \mathbf{i}_M in terms of disturbances to the dynamic system of an industrial robot. Simpson et al. [7] as well investigated a sensorless force estimation method based on measurements of the motor current \mathbf{i}_M and the joint angles \mathbf{q} . The method relies on a dedicated joint model including friction and position dependent torque variations, which are caused by electrical and mechanical effects in the motors and gearboxes. Centripetal, Coriolis and coupling inertia effects have been neglected. The effectiveness of the aforementioned sensorless methods is directly related to the correctness of the underlying dynamics model of the robot including the identified model parameter. Calomé et al. [8] proposed a state observer to estimate the external force-torque vector \mathbf{W} in terms of disturbances to the dynamic systems, which does not rely on an analytical inverse dynamics model. Instead they used the Locally Weighted Projection Regression [9] as a data-driven approach to map the joint angles \mathbf{q} and velocities $\dot{\mathbf{q}}$ to the joint torque $\boldsymbol{\tau}$. The inertia matrix \mathbf{M} is assumed to be known. Smith and Hashtrudi-Zaad [10] adopted this method and modelled the inverse dynamics in terms of an artificial neural network. They directly used the data-driven model as a force observer. Additionally, the influence of joint acceleration $\ddot{\mathbf{q}}$ was investigated, which is obtained as the second derivative of the joint angles \mathbf{q} and therefore prone to noise. Gravity and friction are neglected for the experimental validation with a 3-DOF (degrees of freedom) haptic device. Further, the acquisition of joint torque $\boldsymbol{\tau}$ as the labels for supervised model training is not discussed.

There is a tendency in industrial robots to equip joint axes with double encoders, which means that the primary encoder on the drive side of each axis is accompanied by a secondary encoder on the load side. Commercial examples are the industrial robots M-900iB/700 by the company Fanuc K.K., Oshino, Japan, the MAX-100 by MABI Robotic AG, Veltheim, Switzerland, as well as the industrial robots, which are equipped with double encoders posteriori by Electroimpact, Inc., Mukilteo, USA. The main reason for the usage of double encoders is the increased absolute positional accuracy and overall stiffness of industrial robots [11]. Kaminaga et al. [12] as well as Yamada et al. [13] additionally use self-designed double encoders for joint torque $\boldsymbol{\tau}$ estimation and control. Han et al. [14] further estimated the external force-torque vector \mathbf{W} based on double encoders by using an inverse dynamics model of a 7-DOF robot. All model terms are assumed to be known. They concluded that external force-torque vector \mathbf{W} estimation based on double encoders is feasible in static state, but suffers from severe deviations in the dynamic state.

In this paper the idea described by Han et al. [14] is adopted and relaxed by the fact that a sophisticated dynamic model of the industrial robot is known. Derived from the well-known inverse dynamics equation of industrial robots, the joint effects are separated into two parts. Joint stiffness \mathbf{K}_θ is experimentally determined and modelled by a piecewise linear function. Unknown model terms are captured by a Gaussian Process Regression (GPR).

The remaining paper is structured into four sections. Section 2 describes the hybrid model. Section 3 is dedicated to the model identification. In section 4 experimental validations are performed, before section 5 summarizes the paper.

2. HYBRID MODEL FOR EXTERNAL FORCE-TORQUE ESTIMATION

The proposed hybrid model is derived based on the well-known dynamic model of serial kinematic robots in joint space, which captures the drive torque $\boldsymbol{\tau}$ according to Eq. 1 [15].

$$\boldsymbol{\tau} = \underbrace{\mathbf{M}(\mathbf{q})\ddot{\mathbf{q}}}_{\text{inertia term}} + \underbrace{\mathbf{C}(\mathbf{q},\dot{\mathbf{q}})\dot{\mathbf{q}}}_{\text{Coriolis and centripetal term}} + \underbrace{\mathbf{G}(\mathbf{q})}_{\text{gravitation term}} + \underbrace{\boldsymbol{\tau}_f(\dot{\mathbf{q}})}_{\text{friction term}} + \underbrace{\mathbf{J}(\mathbf{q})^T\mathbf{W}}_{\text{external force-torque term}} \quad (1)$$

In Eq. 1 \mathbf{q} , $\dot{\mathbf{q}}$ and $\ddot{\mathbf{q}}$ are the vector of generalized joint coordinates, velocities and accelerations, respectively, \mathbf{M} is the joint dependent inertia matrix, \mathbf{C} the Coriolis and centripetal coupling matrix, \mathbf{G} the joint dependent torque due to gravitational loading, $\boldsymbol{\tau}_f$ the joint torque due to friction, \mathbf{J} the joint jacobian matrix and \mathbf{W} the external force-torque vector applied to the TCP. The applied drive torque $\boldsymbol{\tau}$ to each robot joint causes an elastic deformation $\Delta\boldsymbol{\theta}$ between the input and output side of the corresponding gearbox due to its limited torsional stiffness \mathbf{K}_θ . In conclusion the drive torque $\boldsymbol{\tau}$ can be modelled as a function of the elastic joint deformations $\Delta\boldsymbol{\theta}$ according to Eq. 2.

$$\boldsymbol{\tau} = f(\Delta\boldsymbol{\theta}) = \mathbf{K}_\theta \cdot \Delta\boldsymbol{\theta} \quad (2)$$

where \mathbf{K}_θ represents the stiffness matrix in joint space.

For simplicity in the remaining paper the static or quasi-static case is considered, where the inertia as well as the Coriolis and centripetal term in Eq. 1 become zero. Combining Eq. 1 with Eq. 2 and rearranging for the elastic deformation $\Delta\boldsymbol{\theta}$ yields Eq. 3.

$$\Delta\boldsymbol{\theta} = \mathbf{K}_\theta^{-1}(\mathbf{G}(\mathbf{q}) + \boldsymbol{\tau}_f(\dot{\mathbf{q}}) + \mathbf{J}(\mathbf{q})^T\mathbf{W}) \quad (3)$$

Eq. 3 can be interpreted as a model capturing the relation between elastic joint deformations $\Delta\boldsymbol{\theta}$ and the external force-torque vector \mathbf{W} . In this context, Eq. 3 has three unknown model terms:

- *Gravitational loading $\mathbf{G}(\mathbf{q})$* : The joint torque due to gravitational loading \mathbf{G} is dependent on the joint angles \mathbf{q} , as the centre of mass shifts when the robot is moved. Typically, it is assumed that the centre of mass of each link is located on the connection line between two consecutive joints and that the gravitational loading of the link is applied partially to the previous and following joint [16]. Based on that, the joint torque caused by gravitational loading \mathbf{G} can be calculated by using the joint jacobian matrix \mathbf{J} . This approach assumes, that the masses m as well as the locations of the centre of masses are known for the whole structure, including the drives, gearboxes, links and auxiliary components. Such information is usually not accessible for commercial industrial robots. In addition, the approach neglects asymmetries in the structure and becomes complex when closed-chain kinematics such as parallelogram-mechanisms and gravity compensators need to be considered.

- *Friction* $\boldsymbol{\tau}_f(\dot{\mathbf{q}})$: Bittencourt et al. [17] presented a dedicated approach to model the joint torque due to friction $\boldsymbol{\tau}_f$ in dependence upon the joint velocity $\dot{\mathbf{q}}$, the total joint loading \mathbf{L} including gravitational and external loading, and the joint temperature \mathbf{T} according to Eq. 4.

$$\boldsymbol{\tau}_f(\dot{\mathbf{q}}, \mathbf{L}, \mathbf{T}) = \boldsymbol{\tau}_l(\mathbf{L}) + \boldsymbol{\tau}_s(\dot{\mathbf{q}}) + \boldsymbol{\tau}_v(\dot{\mathbf{q}}, \mathbf{T}) + \boldsymbol{\tau}_c \quad (4)$$

In Eq. 4 $\boldsymbol{\tau}_l$ denotes the stiction, i. e. static friction at zero joint velocity $\dot{\mathbf{q}}$, $\boldsymbol{\tau}_s$ denotes the Stribeck friction, $\boldsymbol{\tau}_v$ the viscous friction, and $\boldsymbol{\tau}_c$ the Coulomb friction. In the static case considered here the friction $\boldsymbol{\tau}_f$ reduces to the stiction $\boldsymbol{\tau}_s$. Due to backlash, wear and unknown states of contact in terms of lubrication, contact area, surface roughness, etc. all approaches for friction modelling can be considered as simplifications, which rely on a dedicated parameter identification.

- *Joint stiffness matrix* \mathbf{K}_θ : As each robot joint can be modelled as a decoupled single input single output system, the stiffness matrix \mathbf{K}_θ becomes a diagonal matrix with the joint stiffness $k_{\theta,i}$ of each gearbox as the diagonal elements. Wu et al. [18] recently published a review paper about the modelling and identification of the joint stiffness matrix \mathbf{K}_θ . The approaches vary in complexity ranging from linear to non-linear joint stiffness [19, 20]. In general, the six joint stiffness terms k_θ are identified from measurements of the pose \mathbf{p} and the external force-torque vector \mathbf{W} with different joint angles $\boldsymbol{\theta}$ in terms of a least square method. The convergence of the fitting algorithm and the correctness of the identified parameters cannot be guaranteed, especially with increasing complexity of the joint stiffness model.

For industrial robots with double encoders the elastic joint deformations $\Delta\boldsymbol{\theta}$ are directly accessible. Equation 3 can therefore be used to predict the external force-torque vector \mathbf{W} , provided that the gravitational loading \mathbf{G} , friction $\boldsymbol{\tau}_f$ and joint stiffness \mathbf{K}_θ are known. The additional sensor data of the double encoders can further be used to bypass the difficulties as stated above in obtaining the three model terms. The idea is to subdivide the total elastic joint deformation $\Delta\boldsymbol{\theta}$ into an amount $\Delta\boldsymbol{\theta}_1$ caused by gravitational loading \mathbf{G} and friction $\boldsymbol{\tau}_f$ as well as an amount $\Delta\boldsymbol{\theta}_2$ caused by the external force-torque vector \mathbf{W} according to Eq. 5 to Eq. 7.

$$\Delta\boldsymbol{\theta} = \Delta\boldsymbol{\theta}_1 + \Delta\boldsymbol{\theta}_2 = \boldsymbol{\theta}_s - \boldsymbol{\theta} \quad (5)$$

$$\text{with } \Delta\boldsymbol{\theta}_1 = \mathbf{K}_\theta^{-1}(\mathbf{G}(\mathbf{q}) + \boldsymbol{\tau}_f(\dot{\mathbf{q}})) = \boldsymbol{\theta}_{s,0} - \boldsymbol{\theta} \quad (6)$$

$$\Delta\boldsymbol{\theta}_2 = \mathbf{K}_\theta^{-1}\mathbf{J}(\mathbf{q})^T\mathbf{W} = \boldsymbol{\theta}_s - \boldsymbol{\theta}_{s,0} \quad (7)$$

GPR is used to model the elastic joint deformation $\Delta\boldsymbol{\theta}_1$. GPR is well suited to model the complex non-linear relations of friction $\boldsymbol{\tau}_f$ and gravitational loading \mathbf{G} , which could already be shown for robot dynamics and robot stiffness modelling [21, 22]. The joint stiffness in terms of the elastic joint deformation $\Delta\boldsymbol{\theta}_2$ is modelled by a piecewise linear function in order to capture the stiffening behaviour at high loads. At this point it is worth mentioning, that it is straight forward to include the inertia as well as the Coriolis and centripetal term in $\Delta\boldsymbol{\theta}_1$. By doing so a larger dataset for the training phase of the gaussian process model with known and varying joint velocities $\dot{\mathbf{q}}$ and accelerations $\ddot{\mathbf{q}}$ becomes mandatory. The method for external force-torque vector \mathbf{W} estimation based on the hybrid model is summarized in Fig. 1. In the remaining section the GPR as well as the joint stiffness model are explained in detail.

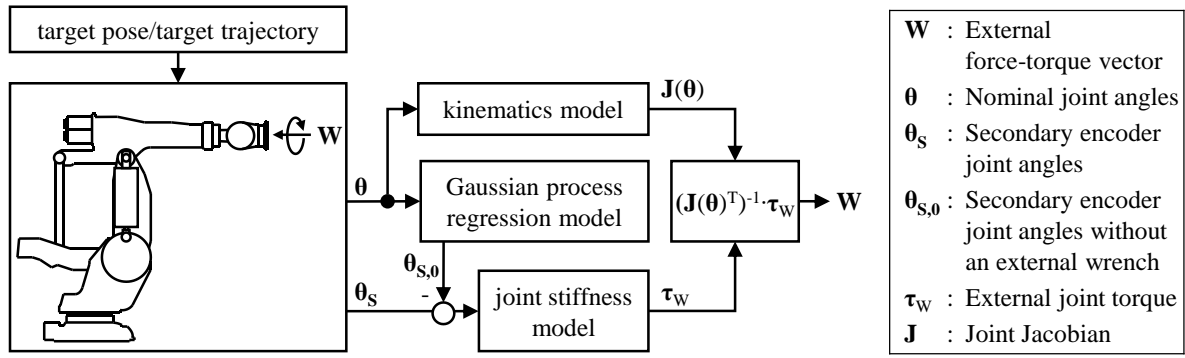


Fig. 1. Summary of the hybrid model for external force-torque vector \mathbf{W} estimation based on double encoders

2.1. GAUSSIAN PROCESS REGRESSION MODEL

An arbitrary dataset $\mathcal{D} = \{\mathbf{x}_i, y_i \mid i = 1, \dots, n\}$ of n observations with \mathbf{x}_i as the input vector and y_i as the corresponding output value is assumed. The goal in a regression problem is to find a function f , which maps the input vector \mathbf{x}_i to the output value y_i according to Eq. 8.

$$y_i = f(\mathbf{x}_i) + \epsilon \quad (8)$$

where ϵ is additive noise and represents the regression error. It is assumed that $\epsilon \sim \mathcal{N}(0, \sigma_n^2)$ follows a Gaussian distribution with zero mean and noise variance σ_n^2 . For a GPR the function f is completely specified by a mean function $m(\mathbf{x})$ and a kernel $k(\mathbf{x}, \mathbf{x}')$ as stated by Eq. 9 to Eq. 11.

$$f \sim \mathcal{GP}(m(\mathbf{x}), k(\mathbf{x}, \mathbf{x}')) \quad (9)$$

$$\text{with } m(\mathbf{x}) = E[f(\mathbf{x})] \quad (10)$$

$$k(\mathbf{x}, \mathbf{x}') = E[(f(\mathbf{x}) - m(\mathbf{x})) (f(\mathbf{x}') - m(\mathbf{x}'))] \quad (11)$$

where the mean function $m(\mathbf{x})$ denotes the expected output of $f(\mathbf{x})$ and the kernel $k(\mathbf{x}, \mathbf{x}')$ the covariance. Typical examples of the mean function $m(\mathbf{x})$ and the kernel $k(\mathbf{x}, \mathbf{x}')$ are stated in Eq. 12 and Eq. 13, where the latter is called squared exponential or radial basis function kernel.

$$m(\mathbf{x}) = 0 \quad (12)$$

$$k(\mathbf{x}, \mathbf{x}') = \sigma_f^2 \cdot \exp\left(-\frac{1}{2} (\mathbf{x} - \mathbf{x}')^T \mathbf{\Lambda}^{-1} (\mathbf{x} - \mathbf{x}')\right) \quad (13)$$

In Eq. 13 σ_f^2 is the signal variance and $\mathbf{\Lambda}$ the diagonal matrix with the length-scale of each input dimension as the diagonal elements. The signal variance σ_f^2 , the length-scale matrix $\mathbf{\Lambda}$ as well as the noise variance σ_n^2 are the so called hyperparameters of GPR, which are tuned in the training phase. One huge advantage of GPR is its non-parametric characteristics, which means that it does not rely on any assumptions about the functional form of f . Due the Bayesian nature of GPR, the model is capable of handling noisy data and gives full predictive distributions of unknown test data \mathbf{x}_* in terms of a posterior Gaussian distribution with mean and covariance according to Eq. 14 and Eq. 15, respectively.

$$\overline{f(\mathbf{x}^*)} = E[f(\mathbf{x}^*)] = m(\mathbf{x}^*) + k(\mathbf{x}^*, \mathbf{x}) \cdot [k(\mathbf{x}, \mathbf{x}) + \sigma_n^2 \mathbf{I}]^{-1} (\mathbf{y} - m(\mathbf{x})) \quad (14)$$

$$\text{cov}[f(\mathbf{x}^*)] = k(\mathbf{x}^*, \mathbf{x}^*) - k(\mathbf{x}^*, \mathbf{x}) \cdot [k(\mathbf{x}, \mathbf{x}) + \sigma_n^2 \mathbf{I}]^{-1} \cdot k(\mathbf{x}, \mathbf{x}^*) \quad (15)$$

Further insights in GPR can be found in great detail in the work of Rasmussen and Williams [21]. In this paper the Statistics and Machine Learning Toolbox of the software MATLAB R2022a by the company The MathWorks Inc., Massachusetts, USA, is used in order to apply GPR to the regression problem stated in Eq. 6. The six nominal joint angles $\boldsymbol{\theta}$ serve as inputs to the GPR. The output is defined by the elastic joint deformations $\Delta\boldsymbol{\theta}_1$, which are given by the difference between the joint angles of the secondary encoders without additional external load $\boldsymbol{\theta}_{s,0}$ and the nominal joint angles $\boldsymbol{\theta}$. As a GPR is a single-output model, six independent models are trained separately for each component of the elastic joint deformation $\Delta\boldsymbol{\theta}_1$. MATLAB's implementation of GPR allows additionally for the optimization of the type of mean and kernel function.

2.2. JOINT STIFFNESS MODEL

The elastic joint deformation $\Delta\boldsymbol{\theta}_2$ caused by the external force-torque vector \mathbf{W} according to Eq. 7 is modelled in terms of the piecewise linear function g given in Eq. 16.

$$g_i(\tau_i) = \Delta\theta_{2,i} = \begin{cases} m_{1,i}\tau_{W,i} + \tau_{Wc1,i} & , \text{ for } \tau_{W,i} < \tau_{W0,i} \\ m_{2,i}\tau_{W,i} & , \text{ for } -\tau_{W0,i} \leq \tau_{W,i} \leq \tau_{W0,i} \\ m_{3,i}\tau_{W,i} + \tau_{Wc3,i} & , \text{ for } \tau_{W,i} \geq \tau_{W0,i} \end{cases} \quad , i = \{1, \dots, 6\} \quad (16)$$

In Eq. 16 m_1 , m_2 and m_3 are the slopes as well as τ_{Wc1} and τ_{Wc3} the additive constants of the piecewise linear functions. The linear segments are separated by the symmetric interval $[-\tau_{W0,i}, \tau_{W0,i}]$, where $\tau_{W0,i}$ is the near-zero load. The external joint torque $\boldsymbol{\tau}_W = (\tau_{W,1}, \dots, \tau_{W,6})^T$ follows from the external force-torque vector \mathbf{W} according to Eq. 17.

$$\boldsymbol{\tau}_W = \mathbf{J}(\mathbf{q})^T \mathbf{W} \quad (17)$$

The implementation of Shape Language Modeling (SLM) in MATLAB by D'Errico [23] is used to identify the piecewise linear function g_i for each joint. In addition, the near-zero load $\tau_{W0,i}$ is identified for each joint such that the root mean squared error (RMSE) of the fitted piecewise linear function is minimized. The minimization is performed based on a bounded particle swarm optimization.

3. EXPERIMENTAL INVESTIGATION AND MODEL IDENTIFICATION

The industrial robot M-900iB/700 by the company Fanuc K.K., Oshino, Japan, as shown in Fig. 2 serves as a demonstrator throughout the paper. The industrial robot has passive, spring-based gravity compensators to reduce the gravitational loading of axis two and three. Further, it is equipped with a parallelogram-mechanism to increase the overall stiffness and maximal payload.

On each axis secondary encoders by the company Renishaw PLC., Wotton-under-Edge, UK, are installed at the output side of the gearboxes. The values of the primary and secondary encoders as well as the nominal joint values can be accessed as system variables in runtime through a TCP/IP (transmission control protocol/internet protocol) connection. The spindle POWERmaster BEX35 by the company Otto Suhner AG, Lupfig, Switzerland, with a nominal power of $P = 9.5$ kW is mounted at the flange of the robot.

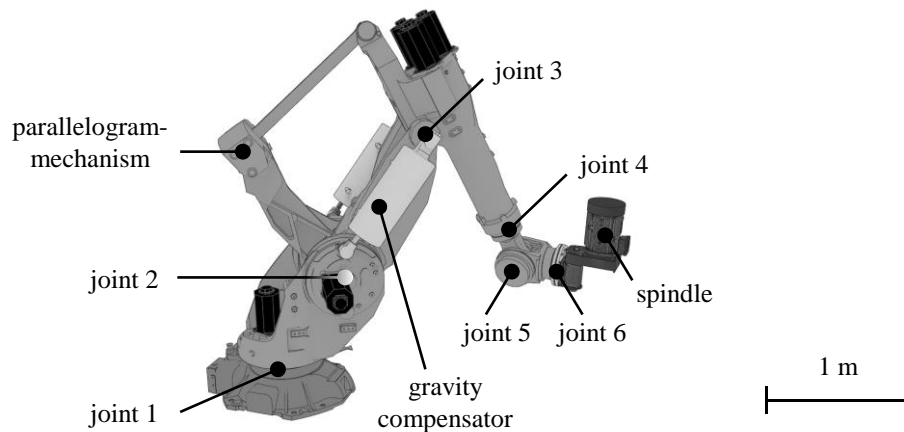


Fig. 2. Industrial Robot M-900Ib/700

3.1. GPR MODEL IDENTIFICATION

To identify a GPR model mapping the nominal joint angles θ to the elastic joint deformations $\Delta\theta_1$ a dataset $\mathcal{D}_i = \{\theta_j, \Delta\theta_{1,i,j} \mid i = 1, \dots, 6; j = 1, \dots, n\}$ need to be experimentally obtained for each output dimension. Therefore, the industrial robot is moved to $n = 1,000$ random joint configurations under consideration of the workspace boundaries. The accessibility of each joint configuration is checked a priori by an inverse kinematic algorithm. Due to the randomness of the joint configurations, it can be guaranteed that backlash in each joint is passed several times. By covering the whole workspace, it is further guaranteed that extreme poses in terms of gravitational and frictional loading of the individual joints are included in the training data, which promotes the learning of these effects. The spindle is assumed to be part of the robot system and is the only payload during the experiments. At each joint configuration the nominal joint angles θ and the values of the secondary encoders $\theta_{s,0}$ are recorded. $N = 960$ datapoints are used to fit the GPR model. With the remaining $N = 40$ datapoints the accuracy of the model is tested as shown in Fig. 3. As can be seen from Fig. 3, the GPR model is capable of predicting the joint deformations $\Delta\theta_1$ accurately. Deviations occur especially for the joints $i = 1$ and $i = 6$. For both joints the gravitational loading \mathbf{G} is (close to) zero. Hence, the effects captured by the GPR model reduce to friction τ_f according to Eq. 6, which is influenced among others by backlash and temperature. To increase the GPR model accuracy in future work, additional dependencies in terms of input parameters can be incorporated. Such input parameters might be the joint approach direction and the joint temperature, in order to capture backlash and the thermal behaviour, respectively. Due to the Bayesian nature of GPR the predictions include not only

the expected mean value, but also the covariance, as described in section 2.1. From the covariance a confidence interval of the predictions can be calculated as shown in Fig. 3 for a 95% confidence interval. For the joints $i = 1$ and $i = 6$ the GPR model “knows” about its uncertainty by means of a wide confidence interval. Such uncertainty information is useful for decision making based on data-driven black box models.

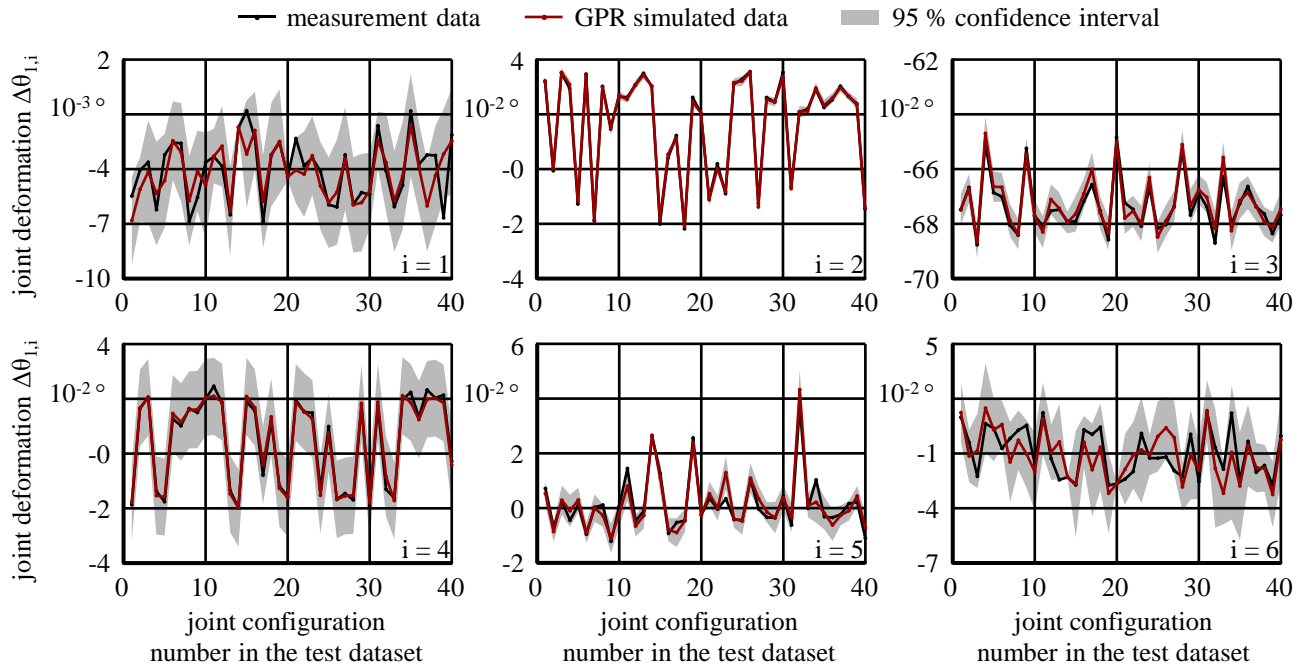


Fig. 3. GPR model performance with unknown test data

3.2. JOINT STIFFNESS IDENTIFICATION

The measurement set-up shown in Fig. 4 a) is used to identify the joint stiffness matrix \mathbf{K}_θ in terms of a piecewise linear function for each joint according to Eq. 16.

An external force \mathbf{F} is applied to a dummy-tool by a screw. The dummy-tool is mounted in the spindle. By rotating the screw stepwise in and out, the external force \mathbf{F} applied to the TCP can be increased and decreased. A loading-unloading-loading-unloading sequence as shown exemplary in Fig. 4b for one joint configuration is performed manually. The external force \mathbf{F} is measured with the dynamometer 9257B by the company Kistler Instrumente AG, Winterhur, Switzerland. The axes of the dynamometer are aligned with the cartesian coordinate system, i. e. the base frame, of the robot by using a measurement gauge. In addition, the yaw and pitch angle of the external force \mathbf{F} can be changed by a rotary table. The measurements are repeated for different joint configurations so that a dominant external joint torque τ_w is applied to each joint for at least one sequence. The joint configurations and force directions are chosen with a trial-and-error approach. For each joint configuration the three components of the external force \mathbf{F} as well as the joint angles of the secondary encoders θ_s are measured as a timeseries, see Fig. 4b. Discrete values are obtained from the timeseries by extracting and averaging of the constant areas.

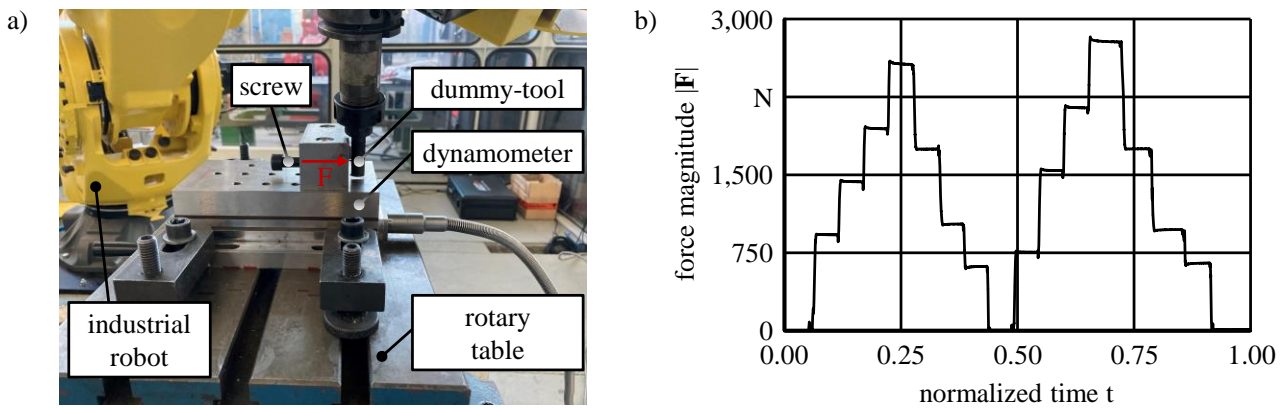


Fig. 4. Experimental investigation of the external force-torque vector \mathbf{W} ;
a) measurement set-up; b) exemplary force signal

Based on Eq. 17 the external joint torque $\tau_{\mathbf{W}}$ follows from the external force-torque vector $\mathbf{W} = (\mathbf{F}^T, \mathbf{0}^T)^T$. The joint deformations $\Delta\theta_2$ are given as the difference between the joint angles of the secondary encoders with and without external loading, θ_s and $\theta_{s,0}$, respectively. The joint deformations $\Delta\theta_2$ and the external joint torque $\tau_{\mathbf{W}}$ are used to identify the piecewise linear function as well as the near zero load $\tau_{\mathbf{W}0}$ according to Eq. 16. Figure 5. shows the experimental results in comparison to the fitted piecewise linear function for each joint. All joints follow a near linear behaviour with a steeper section, i. e. lower joint stiffness k_{θ} , within the near zero load $\tau_{\mathbf{W}0}$ region. The stiffness curves in Fig. 5 do not only show the behaviour of the respective gearboxes, but also the behaviour of the total drive train. For axis three, for example, this includes the stiffness of the parallelogram mechanism, for which reason differences between the axes are reasonable.

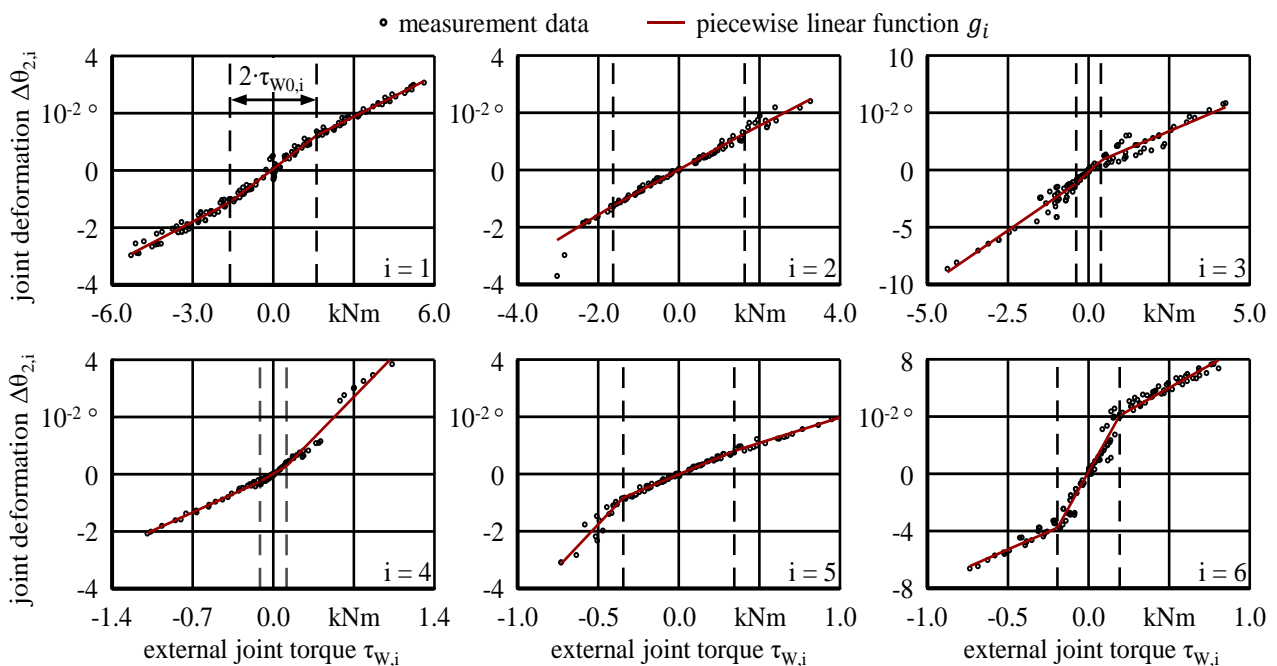


Fig. 5. Joint stiffness model in terms of piecewise linear functions with optimized near zero load interval

4. EXPERIMENTAL VALIDATION

In order to validate the method an experimental set-up according to Fig. 6 is used. A force-torque vector \mathbf{W} is applied to the TCP by an airspring, which is mounted at the one end to a dummy tool of the industrial robot and at the other end to a dynamometer. Both ends are fixed by a ball joint so that circular trajectories can be realized. The nominal joint angles $\boldsymbol{\theta}$ as well as the measured ones from the secondary encoders $\boldsymbol{\theta}_s$ are recorded for $N = 100$ discrete poses along a circular trajectory with a radius of $R = 750$ mm in the X-Y-plane of the industrial robot. To increase the joint movements especially in the wrist the orientation about the global X- and Y-axis of the industrial robot are changed in a sine and cosine manner with a magnitude of $\alpha = 15^\circ$. The experiments are repeated with and without an acting force-torque vector \mathbf{W} , which allows to validate the GPR model as well as the joint stiffness model in terms of the elastic joint deformations $\Delta\boldsymbol{\theta}_1$ and $\Delta\boldsymbol{\theta}_2$, respectively.

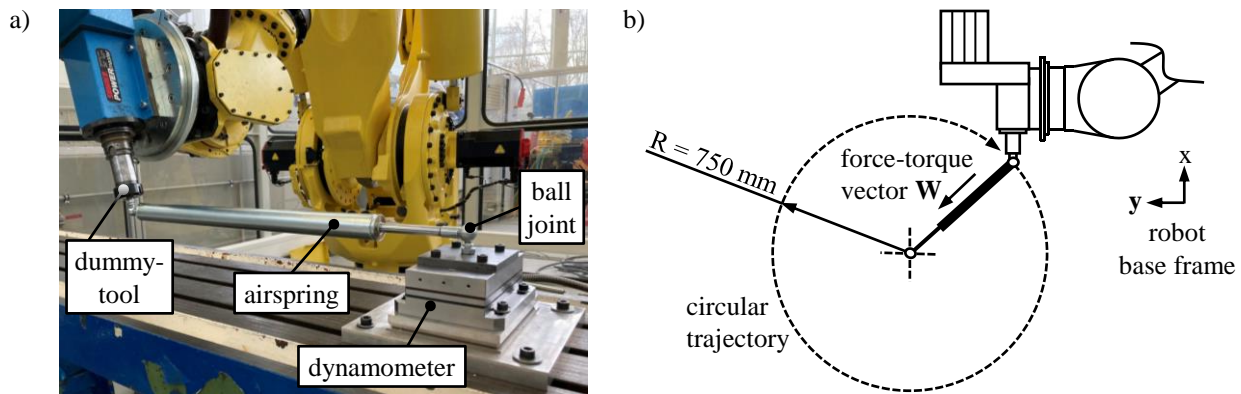


Fig. 6. Experimental validation; a) measurement set-up; b) schematic principle

Figure 7 shows the result of the GPR model for the $N = 100$ poses along the circular trajectory. Even the high frequent changes of joints $i = 2$ and $i = 5$ are captured very accurately. For the joints $i = [1,3,4]$ the GPR model is capable to predict the trends. The highest deviations are observed for joint $i = 6$, which is only slightly loaded by gravity due to the inclination angle of the spindle α . However, trends can still be estimated and the confidence prediction is well calibrated. Fig. 8 shows the estimated external force-torque vector \mathbf{W} in the dominant X- and Y-directions respectively. It can be seen, that the method is valid to predict the shape of the external force-torque vector \mathbf{W} . In more than 50% of the poses the error of the predicted external force-torque vector \mathbf{W} is below 25%. However, in some configurations there are some major deviations in the predicted external force-torque vector \mathbf{W} , which could be caused by the simplification of the joint stiffness as a piecewise linear function. In reality the joint stiffness follows a hysteretic behaviour with differing loading and unloading characteristics. Further, the elastic joint deformation $\Delta\boldsymbol{\theta}_2$ is modelled independent of the pose. Especially in joint $i = 3$ this assumption might be insufficient, as the elastic joint deformation $\Delta\theta_{2,3}$ includes errors of the parallelogram mechanism. In summary, the proposed method can be used to estimate the external force-torque vector \mathbf{W} , which

proves the validity of decomposing the elastic joint deformations $\Delta\theta$ and the corresponding hybrid modelling approach.

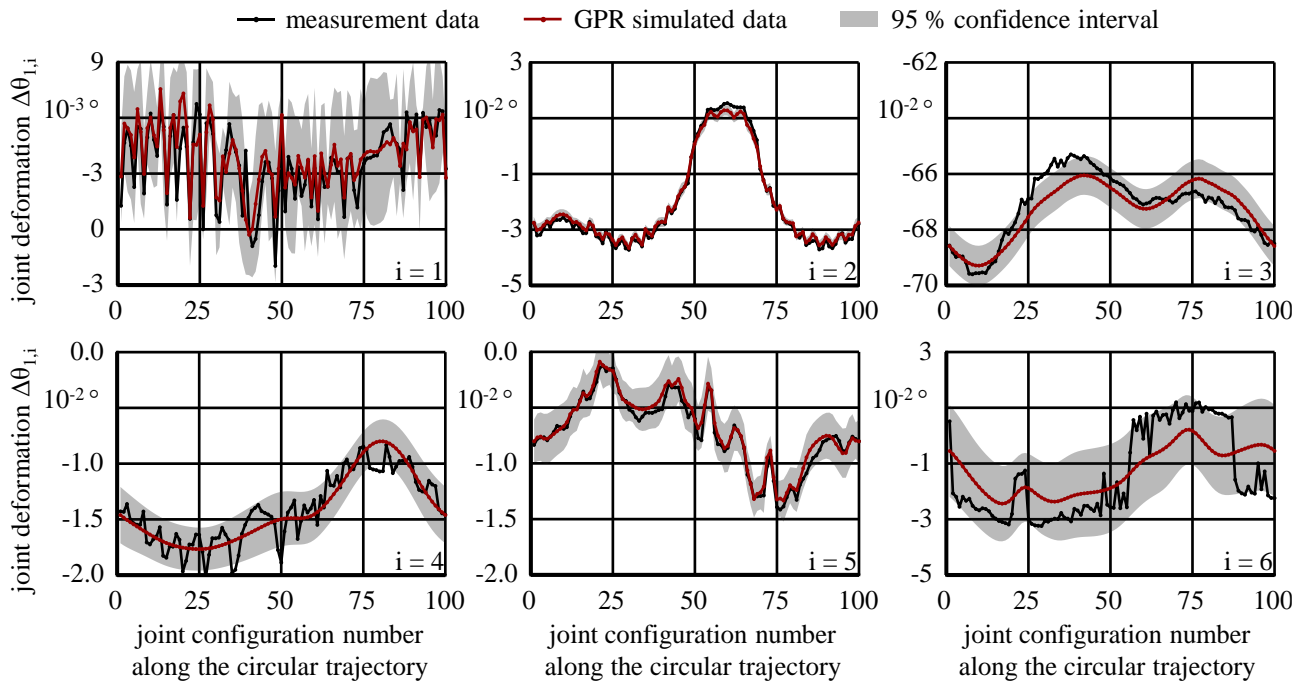


Fig. 7. GPR model performance at $N = 100$ poses along the circular trajectory

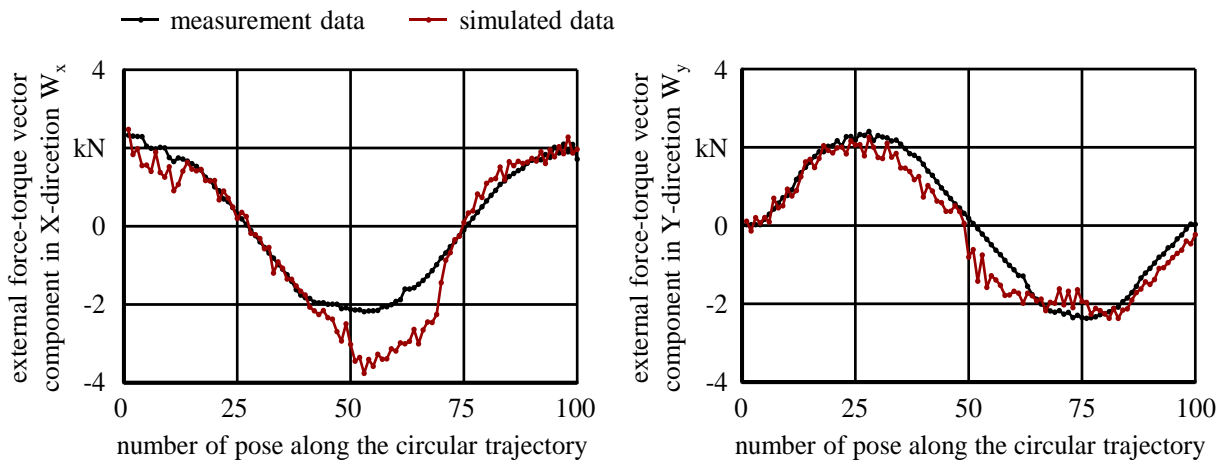


Fig. 8. Comparison of the measured and simulated external force-torque vector \mathbf{W}

5. SUMMARY

Within this paper a hybrid model to predict the external force-torque vector \mathbf{W} based solely on measurements of joint angles θ_s from secondary encoders is proposed. The idea relies on a decomposition of the measured elastic joint deformations $\Delta\theta$, when an external force-torque vector \mathbf{W} is applied to the tool centre point. One part of the elastic joint

deformations caused by gravity and friction $\Delta\theta_1$ is captured by a Gaussian process regression. The other part $\Delta\theta_2$ is directly influenced by the external force-torque vector \mathbf{W} and modelled in terms of piecewise linear functions, which represent the joint stiffness \mathbf{K}_θ . In experimental validations it could be proven that the hybrid model is capable to estimate the external force-torque vector \mathbf{W} . For the majority of robot joint configurations, the accuracy of the predictions is above 75%. Hence, the method can be used in applications as e.g. human-robot collaborations, force control and model-based compensation of tool deflections. By using the proposed hybrid model additional force-torque sensors can be saved, which reduces investment costs and improves robot dynamics as no additional mass is applied to the robot. However, in some joint configurations the hybrid model shows severe deviations, which might be influenced by backlash, hysteretic behaviour and pose dependency of joint stiffness. Incorporating more data in the training of Gaussian Process Regression as well as capturing loading-unloading effects and angular dependency in joint stiffness \mathbf{K}_θ could further improve the method in future work.

REFERENCES

- [1] UHLMANN E., HEITMÜLLER F., MATHEI M., REINKOBER S., 2013, *Applicability of Industrial Robots for Machining and Repair Processes*, Procedia CIRP 11, 234–238.
- [2] VERL A., VALENTE A., MELKOTE S., BRECHER C., OZTURK E., TUNC L.T., 2019, *Robots in Machining*, CIRP Annals – Manufacturing Technology, 68, 799–822.
- [3] CAO M.Y., LAWS S., RODRIGUEZ Y., BAENA F., 2021, *Six-Axis Force/Torque Sensors for Robotics Applications: A Review*, IEEE Sensors Journal, 21/24, 27238–27251.
- [4] PHONG L.D., CHOI J., KANG S., 2013, *External Force Estimation Using Joint Torque Sensors and its Application to Impedance Control of a Robot Manipulator*, 13th International Conference on Control, Automation and Systems, 1794–1798.
- [5] MURAKAMI T., NAKAMURA R., YU F., OHNISHI K., 1993, *Force sensorless impedance control by Disturbance Observer*, Conference Record of the Power Conversion Conference, 352–357.
- [6] QIN J., LEONARD F., ABBA G., 2013, *Experimental External Force Estimation Using a Non-Linear Observer for 6 axes Flexible-Joint Industrial Manipulators*, 9th Asian Control Conference, 1–6.
- [7] SIMPSON J.W.L., COOK C.D., LI Z., 2002, *Sensorless Force Estimation for Robots with Friction*, Proceedings of Australasian Conference on Robotics and Automation, 94–99.
- [8] CALOME A., PARDO D., ALENYA G., TORRAS C., 2013, *External Force Estimation During Compliant Robot Manipulation*, IEEE International Conference on Robotics and Automation, 3535–3540.
- [9] VIJAYAKUMAR S., SCHAAL S., 2000, *Locally Weighted Projection Regression: An $O(n)$ Algorithm for Incremental Real Time Learning in High Dimensional Space*, 17th International Conference on Machine Learning, 1079–1086.
- [10] SMITH A.C., HASHTRUDI-ZAAD K., 2005, *Application of Neural Networks in Inverse Dynamics Based Contact Force Estimation*, IEEE Conference on Control Applications, 1021–1026.
- [11] KLIMCHIK A., PASHKEVICH A., 2018, *Robotic Manipulators with Double Encoders: Accuracy Improvement Based on Advanced Stiffness Modeling and Intelligent Control*, IFAC-PapersOnLine, 11/51, 740–745.
- [12] KAMINAGA H., ODANAKA K., KAWAKAMI T., NAKAMURA Y., 2011, *Measurement Crosstalk Elimination of Torque Encoder Using Selectively Compliant Suspension*, IEEE International Conference on Robotics and Automation, 4774–4779.
- [13] YAMADA S., INUKAI K., FUJIMOTO H., 2015, *Joint Torque Control for Two-Inertia System with Encoders on Drive and Load Sides*, IEEE 13th International Conference on Industrial Informatics, 396–401.
- [14] HAN Z., YUAN J., GAO L., 2018, *External Force Estimation Method for Robotic Manipulator Based on Double Encoders of Joints*, IEEE International Conference on Robotics and Biomimetics, 1852–1857.
- [15] CORKE P., 2016, *Robotics, Vision and Control – Fundamental Algorithms in MATLAB*, Springer International Publishing AG, Cham, Switzerland.

- [16] KLIMCHIK A., 2011, *Enhanced Stiffness Modelling of Serial and Parallel Manipulators for Robotic-Based Processing of High Performance Materials*, PhD thesis, Ecole Centrale de Nantes.
- [17] BITTENCOURT A.C., WERNHOLT E., SANDER-TABALLAEY S., BORGARDH T., 2010, *An Extended Friction Model to Capture Load and Temperature Effects in Robot Joints*, IEEE/RSJ International Conference on Intelligent Robots and Systems, 6161–6167.
- [18] WU K., LI J., ZHAO H., ZHONG Y., 2022, *Review of Industrial Robot Stiffness Identification and Modelling*, Applied sciences, 12/8719, 1–24.
- [19] ABELE E., ROTHENBÜCHER S., WEIGOLD M., 2008, *Cartesian Compliance Model for Industrial Robots Using Virtual Joints*, Production Engineering – Research and Development, 2, 339–343.
- [20] SCHNEIDER U., MOMENI-K M., ANSALONI M., VERL A., 2014, *Stiffness Modeling of Industrial Robots for Deformation Compensation in Machining*, IEEE/RSJ International Conference on Intelligent Robots and Systems, 4464–4469.
- [21] RASMUSSEN C.E., WILLIAMS K.I., 2006, *Gaussian Processes for Machine Learning*, the MIT Press, Massachusetts.
- [22] BLUMBERG J., LI Z., BESONG L.I., POLTE M., BUHL J., UHLMANN E., BAMBACH M., 2021, *Deformation Error Compensation of Industrial Robots in Single Point Incremental Forming by Mean of Data-Driven Stiffness Model*, 26th International Conference on Automation and Computing, 1–6.
- [23] D'ERRICO J., 2023, *SLM-Shape Language Modeling*, MATLAB Central File Exchange.